Published in final edited form as:
NMR Biomed. 2011 February ; 24(2): 216–223. doi:10.1002/nbm.1576.

MRI of retinal and choroidal blood flow with laminar resolution

Eric R. Muir[a,b] and **Timothy Q. Duong**[a,c,d,*]

[a]Research Imaging Center, Departments of Ophthalmology, Radiology and Physiology, University of Texas Health Science Center, San Antonio, TX, USA

[b]Department of Biomedical Engineering, Georgia Institute of Technology, Atlanta, GA, USA

[c]South Texas Veterans Health Care System, San Antonio, TX, USA

[d]Southwest National Primate Research Center, San Antonio, TX, USA

Abstract

The retina is nourished by two distinct circulations: the retinal vessels within the inner retina and the choroidal vessels behind the neural retina. The outer nuclear layer and the inner and outer segments of the photoreceptors in between are avascular. The aim of this study was to determine whether arterial spin labeling MRI could provide sufficient resolution to differentiate between quantitative retinal blood flow (rBF) and choroidal blood flow (chBF), and whether this technique is sufficiently sensitive to detect vascular-specific blood flow (BF) changes modulated by anesthetics. Arterial spin labeling MRI was performed at 42 × 42 × 400 μm^3 in the mouse retina at 7 T, and was used to investigate the effects of isoflurane and ketamine/xylazine anesthesia on rBF and chBF. MRI yielded unambiguous differentiation of rBF, chBF and the avascular layer in between. Under isoflurane, chBF was 7.7 ± 2.1 mL/g/min and rBF was 1.3 ± 0.44 mL/g/min (mean ± SD, $n = 7$, $p < 0.01$). Under ketamine/xylazine anesthesia in the same animals, chBF was 4.3 ± 1.9 mL/g/min and rBF was 0.88 ± 0.22 mL/g/min ($p < 0.01$). Under ketamine/xylazine anesthesia, rBF was lower by 29% ($P < 0.01$) and chBF by 42% ($P < 0.01$) relative to isoflurane. This study demonstrates, for the first time, the quantitative imaging of rBF and chBF *in vivo*, providing a new method to study basal values and alterations of rBF and chBF.

Keywords

perfusion; arterial spin labeling (ASL); high-resolution MRI; isoflurane; ketamine; xylazine; retinal diseases; ophthalmology

INTRODUCTION

The retina consists of multiple structured layers and is nourished by two separate blood supplies: the retinal and choroidal circulations, located on either side of the retina (1). Starting from the vitreous, the anatomical layers of the neural retina include the ganglion cell layer, inner plexiform layer, inner nuclear layer, outer plexiform layer, outer nuclear layer, and inner and outer segments. Behind these layers are the retinal pigment epithelium, choroid and sclera. The neural retina and choroid together are only about 250 μm thick in rodents (2,3). Retinal vessels are mainly localized on the inner surface of the retina, with arterioles and capillaries projected into the ganglion cell layer, inner plexiform layer and

*Correspondence to: T. Q. Duong, Research Imaging Center, University of Texas Health Science Center at San Antonio (UTHSCSA), 8403 Floyd Curl Dr., San Antonio, TX 78229, USA. duongt@uthscsa.edu.

inner nuclear layer. The choroidal vessels are located external to the neural retina in the choroid. The outer nuclear layer and the inner and outer segments – located in between the retinal and choroidal vascular layers – are without blood vessels. There are substantial differences in basal blood flow (BF) and BF regulation between the two blood supplies. Choroidal blood flow (chBF) is many times greater than retinal blood flow (rBF), which is similar to cerebral BF (1,4,5). The two vasculatures also respond differently to various BF-regulating factors (6–8).

There is evidence that the two circulations may have different susceptibility to diseases and their deterioration may progress differently. For example, in a cat model of retinitis pigmentosa, rBF is severely compromised, whereas chBF is not affected significantly relative to controls (9). In diabetic retinopathy, the choroidal and retinal blood vessels are anatomically abnormal, and the blood velocity decreases in retinal vessels in the early phase in streptozotocin-induced diabetic rat retina (10,11). Imaging technologies that can quantify noninvasively baseline and dynamic changes of rBF and chBF separately *in vivo* may help to better understand how these two vascular layers are affected, improving the understanding of disease pathophysiology *in vivo*. However, the resolution of rBF and chBF is challenging because of the thin retina.

BF to the retina has been studied using destructive microsphere techniques in animals (4,5,8,9,12,13). The *in vivo* qualitative BF index from the entire retinal thickness of combined retinal and choroidal layers has been reported using optical techniques, such as laser Doppler flowmetry (6) and laser speckle imaging (14). Blood velocity can be measured on surface vessels using optical methods, such as fluorescein angiography (15). Blood velocity can also be measured in retinal and choroidal blood vessels using optical coherence tomography (16). Optical techniques are generally qualitative or the signals are measured from individual blood vessels, which may not accurately reflect local tissue perfusion. In addition, distinguishing BF in the retinal or choroidal vessels using optics is difficult because of the lack of depth resolution with most techniques. Moreover, optical techniques require an unobstructed light path, so eye diseases, such as vitreal hemorrhage and cataract, may preclude the use of optical techniques.

MRI provides noninvasive *in vivo* structural, physiological and functional information without depth limitation and has wide-spread preclinical and clinical applications. Quantitative BF can be imaged with MRI using an exogenous intravascular contrast agent (referred to as dynamic susceptibility contrast MRI) or by magnetically labeling endogenous water in blood [referred to as arterial spin labeling (ASL) MRI] (17). ASL is widely utilized to measure quantitative basal BF and dynamic BF changes associated with functional stimulations in the brain (17). The main drawback of MRI, in general, relative to optical techniques is that it has a lower spatial resolution and a lower signal-to-noise ratio.

In recent years, high-resolution laminar-specific imaging of the retina has been reported. Anatomical MRI yielded a layer-specific structure of the retina (2,18,19). Blood oxygenation level-dependent functional MRI (BOLD fMRI) detected changes associated with physiological stimulations (2), and manganese-enhanced MRI showed differences between light- and dark-adapted retina (19). Disease-induced changes in retinal thicknesses and retinal responses to physiological challenges have been detected by anatomical and BOLD fMRI in rats with retinal degeneration (2). In contrast with anatomical MRI and BOLD fMRI, the signal-to-noise ratio of BF MRI is two orders of magnitude lower, in part because the blood volume in the central nervous system averages 3–5% of the total tissue volume. Although BF MRI in the rat retina has been demonstrated recently, it did not have sufficient spatial resolution to distinguish the two vascular layers of the retina (20,21).

In this study, high-resolution ASL MRI was utilized to image quantitative, layer-specific rBF and chBF in the mouse retina at $42 \times 42 \times 400\ \mu m^3$ resolution at 7 T. BF was measured using the novel cardiac spin labeling technique (22) and a high-performance gradient. The cardiac spin labeling technique is based on the continuous ASL BF technique with a separate labeling coil placed at the heart position (instead of the neck position) to avoid saturation of the imaging slice given the small mouse size. The high-performance gradient affords the use of a very small field of view to enhance high spatial resolution with minimal echo time and data readout time. Moreover, the effects of two anesthetics – isoflurane [a cerebral vasodilator (23)] and ketamine/xylazine [a cerebral vasoconstrictor (24,25)] – on rBF and chBF were also investigated.

MATERIALS AND METHODS

Animal preparation

All animal experiments were performed with institutional approval and in accordance with the Statement for the Use of Animals in Ophthalmic and Vision Research. Experiments were performed on C57BL/6 mice (four female, three male; 5–11 weeks old; 17–28 g; $n = 7$). Animals were first anesthetized with 5% isoflurane, put into a head holder with ear and tooth bars, and placed in an animal holder with a built-in labeling radiofrequency coil and a circulating warm water pad. A 30-gauge needle was inserted in the intraperitoneal space of the animal and extended via PE-10 tubing to outside the scanner for drug administration without moving the animal during MRI. Imaging was performed first under 1.1% isoflurane and spontaneous breathing conditions. In the same animals, anesthesia was subsequently switched to ketamine/xylazine (100 mg/kg–10 mg/kg, intraperitoneally) and isoflurane was discontinued. MRI was repeated approximately 10 min after switching the anesthetics. Air and oxygen were mixed to provide 30% O_2 to the animals during imaging under both anesthetics. MRI under isoflurane was performed first in all mice because its half-life is much shorter than that of ketamine/xylazine, allowing the two anesthetics to be studied in the same animals in the same setting within a reasonable time, thereby reducing intersubject variation. The respiration rate, recorded continuously via a force transducer, was approximately 115 breaths/min under isoflurane and approximately 95 breaths/min under ketamine/xylazine. The rectal temperature was monitored continuously and maintained at 37 ± 0.5°C. Mice were prepared in a lit room before being transferred to the MRI room, in which the lights were turned off. Lighting conditions were not changed during the duration of imaging. In addition, some mice ($n = 4$) were sacrificed in the scanner after *in vivo* experiments with sodium pentobarbital (250 mg/kg, intraperitoneally), and BF imaging was repeated a few minutes after respiration ceased.

MRI methods

MRI studies were performed on a 7-T/30-cm horizontal magnet and a 150-G/cm BGA6S gradient insert (Bruker, Billerica, MA, USA). For imaging, a small circular surface eye coil with active decoupling (internal diameter, 0.6 cm) was placed over the left eye. A circular labeling coil (internal diameter, 0.8 cm) was placed at the heart position for a cardiac spin labeling technique as described previously (22). The two coils were separated by 2.3 cm from center to center.

BF MRI was acquired using two-coil continuous ASL with an echo planar imaging (EPI) sequence. Paired images, one with and one without labeling, were acquired in an interleaved fashion. ASL employed a 2.94-s square radiofrequency pulse to the labeling coil in the presence of a 2.0-G/cm gradient along the flow direction with a post-label delay of 10 ms. The sign of the frequency offset was switched for nonlabeled images. Images were acquired in a coronal orientation with a single slice passing through the retina just below the optic

nerve head, with the slice angled perpendicular to the retina. Two-segment, gradient-echo EPI was used with a field of view of 6.0 × 6.0 mm^2, matrix of 144 × 144 (resolution, 42 × 42 μm^2), a single 0.4-mm slice, TR = 3.0 s per segment and TE = 13 ms. For each scan, 75 pairs of images were typically acquired in a time series (to be averaged offline) with a total acquisition time of 15 min.

Data analysis

Image analysis was performed using codes written in Matlab (Math-Works Inc., Natick, MA, USA), STIMULATE software (University of Minnesota, USA) and Statistical Parametric Mapping (SPM) software. Images were zero-padded to 256 × 256 (nominal resolution, 23 × 23 μm^2) before subsequent processing. All images from each scan were acquired as a time series, aligned using the spatial realignment function in SPM5 and averaged offline.

BF images of the eye S_{BF}, in units of (mL blood)/(g tissue)/min, were calculated pixel by pixel using $S_{BF} = \lambda/T_1 \{(S_{NL} - S_L)/[S_L + (2\alpha - 1)S_{NL}]\}$ (22), where S_{NL} and S_L are the signal intensities of the nonlabeled and labeled images, respectively.λ, the tissue–blood partition coefficient of water, was taken to be 0.9, the same as in the brain (26).λ, a difficult measurement, has not been reported for the retina or choroid. The retinal and choroidal T_1 at 7 T was taken to be 1.8 s (27), which is similar to brain T_1. The labeling efficiency α was measured previously to be 0.7 (22).

BF intensity profiles across the retinal thickness were obtained from BF images by radially projecting lines perpendicular to the retina (2) with profiles obtained at 4 × spatial interpolation. BF profiles were averaged along the length of the retina. Measurements of peak values and layer thicknesses – defined as the half-height width of the peaks – were determined from the average BF profiles for each animal. Because there was no BF post-mortem, BF measurement was made by aligning post-mortem anatomical profiles to the profiles obtained under isoflurane. The locations of rBF and chBF peaks were determined from the isoflurane BF profile. Post-mortem rBF and chBF were then measured from the post-mortem BF profile by averaging over nine points centered at the respective BF peak. Group-average data were tabulated and expressed as the mean ± standard deviation (SD). All statistical analyses used two-sided, paired *t*-tests with $p < 0.05$ indicating statistical significance, unless otherwise specified.

RESULTS

With a resolution of 42 × 42 × 400 μm^3, two distinct BF layers in the retina were resolved, separated by a region of no BF contrast (Fig. 1A). The outer BF layer, which corresponds to the choroid, had very high BF. The inner BF layer, which corresponds to the retinal vessels, had substantially lower BF than the choroid. The middle layer, with little to no BF contrast, corresponds to the avascular region – made up of the outer nuclear layer and the outer and inner photoreceptor segments. BF signals in the ciliary bodies and extra-ocular tissue were also detected sometimes, although not clearly or consistently because of susceptibility-induced signal dropout in the anterior regions of the eye. No statistically significant BF signal was detected in the vitreous or lens ($p > 0.05$, one-sample *t*-test comparing the sample mean to zero, $n = 7$). Figure 1B shows a BF image obtained from the same mouse post-mortem. No BF contrast was detected in the dead animal ($p > 0.05$ for both rBF and chBF, one-sample *t*-test comparing the sample mean to zero, $n = 4$), suggesting that BF was the source of signals *in vivo*. The BF profiles in Fig. 1C show two BF layers distinctly separated by an avascular region in the live mouse and the absence of BF contrast in the dead mouse retina.

Layer-specific BF measurements were made under isoflurane (Fig. 2A) and ketamine/xylazine (Fig. 2B). Group-averaged BF profiles under each anesthetic are shown in Fig. 2C. rBF and chBF were both substantially lower under ketamine/xylazine relative to isoflurane. Table 1 summarizes the peak rBF and chBF values under each anesthetic. BF under ketamine/xylazine was 42% lower in the choroid ($p < 0.01$, $n = 7$) and 29% lower in retinal vessels ($p < 0.01$), relative to isoflurane. The ratio of chBF : rBF was 6.3 under isoflurane and 4.8 under ketamine/xylazine, suggesting that these anesthetics affect rBF and chBF differently. The magnitudes of the changes in chBF and rBF between anesthetics, −3.4 and −0.42 mL/g/min, respectively, were significantly different from each other ($p < 0.05$).

Linear regression analysis showed no statistically significant differences over 15 min of imaging time ($n = 5$, $p > 0.05$ for rBF and chBF under isoflurane and ketamine/xylazine). The group-averaged SDs across acquisition time for isoflurane were 0.22 and 0.53 mL/g/min for rBF and chBF, respectively. The group-averaged SDs across time for ketamine/xylazine were 0.33 and 0.36 mL/g/min for rBF and chBF, respectively. These findings support the stability of ASL BF MRI and animal physiology.

Based on the BF profiles, the thicknesses of the retinal and choroidal vascular layers and the avascular layer in between were estimated (Table 2). The average thickness of the retina, including the choroid, was about 249 μm under isoflurane and ketamine/xylazine ($p > 0.05$, $n = 7$). The distances between the rBF and chBF peaks were 170 μm (isoflurane) and 161 μm (ketamine/xylazine) ($p > 0.05$).

DISCUSSION

This study demonstrates noninvasive, high-resolution, quantitative measurements of rBF and chBF in the mouse retina *in vivo*. This was made possible by the novel cardiac spin labeling BF MRI and a high-performance gradient. chBF was many times higher than rBF. In addition, rBF was 29% lower and chBF was 42% lower under ketamine/xylazine relative to isoflurane. This approach provides reliable quantification of rBF and chBF, as well as the detection of differences between the two anesthetics. ASL BF MRI measurement is noninvasive (which allows longitudinal monitoring of disease progression *in vivo*), quantitative (which facilitates comparison across experimental groups) and depth resolved with high spatial resolution (which allows the unambiguous resolution of rBF and chBF). This novel application of BF MRI could serve as a valuable imaging tool to study rBF and chBF regulation in normal retina and perturbations in retinal diseases in a longitudinal fashion.

Movement and partial-volume effect

Potential hardware drift and eye movement artifacts associated with MRI of the retina have been addressed in detail elsewhere (28). In contrast with previous studies of the rat retina, in which paralytics were found to be needed in addition to isoflurane (2,28), in this study, eye movement in isoflurane-anesthetized mice was considerably lower, and therefore paralytics were unnecessary. Any small motion that occurred over prolonged scans was tolerable and effectively corrected by image alignment. Although both isoflurane and ketamine/xylazine were effective in minimizing eye movement in mice, ketamine/xylazine yielded more stable images than isoflurane in the same animals, probably because xylazine is also a muscle relaxant (24).

The in-plane resolution of $42 \times 42\ \mu m^2$ (before zero filling and interpolation) had approximately six pixels across the entire retina and choroid. This spatial resolution was sufficient to clearly differentiate BF between the retinal and choroidal vascular layers. In the slice thickness direction, the partial-volume effect caused by the curvature of the retina from

a slice thickness of 0.4mmwas estimated to be 12 μm, or less than 5% of the total retinal thickness, assuming a spherical mouse eye of 3.3mm in diameter and a retina 270 μm thick (combined neural retina and choroid).

BF calculation

The ASL technique for imaging the retina and choroid contains some assumptions and limitations. The blood–tissue partition coefficient (λ) of the brain (26) was used in the BF calculations because the blood–tissue partition coefficients in the retina and choroid have not been measured. This is a reasonable assumption for the retina because it is a neural tissue and has similar BF and water content to gray matter (26,29). In this study, we did not consider the effect of transit time on BF measurements. In rats, transit time to the brain is short, approximately 200 ms, and, in mice, the transit time is expected to be shorter. In addition, the labeling efficiency used was measured at the brain (22), modeling the transit delay effects as a modulation of labeling efficiency. However, there could be a slight transit time difference between the two anesthetics which may cause some error in BF comparison, although we do not expect this to be significant in mice. In some disease states, such as vascular occlusive diseases, the effect of the transit time could be significant and would need to be corrected using appropriate post-labeling delays. Previous measurements have shown that retinal T_1 is similar to brain T_1 at 7 T (27). It has also been reported at 11.7 T that retinal and choroidal T_1 are similar to brain T_1 (3). T_2 and the apparent diffusion coefficient of the retina have also been reported to be similar to those of the brain in cats (18). BF errors from λ and T_1 inaccuracies are likely to be small and cause only a linear offset, which affects measurement accuracy but not precision. As such, reliable comparison across experimental groups can be made if the experimental settings are similar.

Thickness measurements from BF data

Precise comparison between MRI and histology is not possible because of the limited in-plane resolution of 42 μm. In addition, images acquired with EPI showed noticeable geometric distortion which probably introduces a small error in thickness measurements. MRI thicknesses should still provide a reasonable estimate when compared with histology. In this study, the neural retina (including the rBF layer and avascular layer) determined by BF MRI was about 171 μm. The neural retina has been reported to be 182 μm in mice (3) and 180 μm in rats (2) by anatomical MRI. Histological thickness measurements of the neural retina were 176–223 μm in mice (3,30,31) and 169 μm in rats (2). The neural retinal thicknesses in mice and rats from MRI and histology are in reasonably good agreement.

The choroidal thickness was 78 μm by BF MRI, consistent with the choroidal thickness of 86 μm reported in rats (2), although somewhat thicker than the value of 52 μm reported in mice (3) with anatomical MRI. The choroidal thickness measured by histology is 15–28 μmin mice (3,31) and 37 μmin rats (2), thinner than the MRI-measured thicknesses. Similar differences have been noted in humans between *in vivo* measurements of choroidal thickness using optical coherence tomography (32) compared with histological measurements (33). Possible explanations for this difference include partial-volume effects from the limited MRI spatial resolution, histological shrinkage and collapse of choroidal vessels after being removed from the systemic circulation for histology. The peak-to-peak distances between the rBF and chBF profiles were 170 and 161 μm in this study, under isoflurane and ketamine/xylazine, respectively, comparable with the peak-to-peak distance of 162 μm in rats measured by anatomical MRI (2).

Quantitative rBF and chBF

Under isoflurane, rBF was 1.3 mL/g/min and chBF was 7.7 mL/g/min. Under ketamine/xylazine, rBF was 0.88 mL/g/min and chBF was 4.3 mL/g/min. rBF and chBF have been

reported using destructive techniques, including microspheres, autoradiography, krypton-85 washout and hydrogen clearance methods. Table 3 summarizes the results from these methods in various species and experimental conditions. Values of rBF have been shown to range from 0.12 to 3.73 mL/g/min, whereas chBF values vary in the range 2–18.98 mL/g/min. The MRI BF measurements in this study fall somewhere in the middle of these reported ranges.

These comparisons show that rBF and chBF measurements vary over a wide range. Factors that could contribute to this spread include differences in species, anesthetics and methodologies. The extent of the retinal vasculature varies widely in mammals, with some species completely lacking this vascular layer (1,34), giving rise to large species' differences. As demonstrated, different anesthetics and dosages have marked effects on BF (20). MRI BF measurements contain certain assumptions, as described above. The size and dose of microspheres can also have a significant effect on the measurement of rBF and chBF (35). BF in the eye measured by microspheres is often given in units of μL blood/min/whole tissue. Conversion to mL/g/min requires the weight of the whole neural retina and whole choroid. Such conversion could introduce inaccuracies in quantitative values through the dehydration of tissue before weighing, difficulty separating the whole retina and choroid from other tissues, and the use of the entire retinal weight when the retinal vessels only perfuse the inner retina (8,9).

Regardless of the experimental conditions or units, chBF has been consistently reported to be many times higher than rBF (1,8,9,26,36,37), with the chBF : rBF ratios ranging from seven (36) to 80 (38). In this study, MRI measured chBF to be 6.3 times larger than rBF under isoflurane and 4.8 times larger than rBF under ketamine/xylazine, most consistent with findings using the krypton-85 washout method (36). These results are also consistent with an MRI study using an intravascular contrast agent (gadolinium diethylenetriaminepentaacetate), which enhanced the choroidal vascular layer more than the retinal vascular layer (2). A higher chBF also agrees with a previous MRI study which reported combined rBF and chBF in rats, at a resolution that was insufficient to resolve the retinal and choroidal vascular layers, as 6.3 ± 1.0 mL/g/min under 1% isoflurane and similar experimental conditions to those used here (20).

Table 3 also summarizes cerebral BF data measured in the same animals, in addition to rBF and chBF. By comparison, chBF is many times higher than cerebral BF, whereas rBF is similar to cerebral BF. Cerebral BF has been reported to be 0.86– 1.27 mL/g/min in rats (17) and 1.1 mL/g/min in mice (22) under 1% isoflurane, similar to rBF (1.3 mL/g/min) but much lower than chBF (7.7 mL/g/min) measured here. Together, these comparisons support the validity of ASL BF MRI measurements in the retina and choroid.

Effects of different anesthetics

Isoflurane is a known vasodilator. BF under isoflurane is higher than BF in awake conditions in the brain (17,23), and a higher isoflurane concentration yields higher cerebral BF up to 2% isoflurane (17,23). In the rat retina, total BF (combined rBF and chBF) under 1.5% isoflurane was 48% higher than that under 1.0% isoflurane (20), showing similar effects as in the brain. In contrast, ketamine/xylazine is known to cause vasoconstriction and has been shown to yield 25–65% lower cerebral BF compared with isoflurane, depending on the brain region (25).

Both rBF and chBF were higher under isoflurane than under ketamine/xylazine, consistent with these anesthetic effects in the brain. This probably represents the combined effect of the removal of vasodilatory isoflurane and the addition of vasoconstrictive ketamine/xylazine. chBF under ketamine/xylazine was 42% lower, but rBF under ketamine/xylazine was only

29% lower, compared with isoflurane. These changes could be a result of systemic effects of the anesthetics, or local effects, which could explain the large BF difference in the choroid.

Systemic respiratory, cardiovascular or metabolic differences between the two anesthetics could account for these global BF differences. The respiration rate was lower under ketamine/xylazine than under isoflurane, which could potentially result in a lower partial pressure of arterial oxygen (P_aO_2) and a higher partial pressure of arterial carbon dioxide (P_aCO_2) (24,25). These changes could not explain the lower BF under ketamine/xylazine because they should increase BF. Ketamine/xylazine does not have a significant effect on blood pressure relative to isoflurane in rats (25), but xylazine has been reported to cause an initial hypertension followed by a return to normal or low blood pressure (24).

Xylazine could affect rBF and chBF differently. Xylazine is an α_2-agonist which binds central and peripheral α_2-adrenoreceptors in the sympathetic nervous system (24). The choroid contains sympathetic nerves which can induce vasoconstriction (39–41), whereas retinal vessels lack direct sympathetic innervation (40,41). This could explain why ketamine/xylazine reduced chBF more than rBF.

Other studies also support the hypothesis that rBF and chBF are regulated differently in some ways. Hyperoxia has little effect on chBF, as measured by laser Doppler flowmetry in the human macula (6). Oxygen electrode measurements showed differential tissue pO_2 responses in the two vascular layers when challenged with hyperoxia and carbogen (42). Interestingly, in the cat eye, halothane caused rBF to increase and chBF to decrease (4). A BOLD fMRI study also suggested differential responses to hyperoxia and hypercapnia in the two vascular layers (2).

CONCLUSIONS

This study has demonstrated the unambiguous resolution of quantitative rBF and chBF *in vivo* by high-resolution MRI. The BF MRI approach is capable of detecting the effects of isoflurane and ketamine/xylazine anesthesia on rBF and chBF. MRI has the potential to provide information on the unique rBF and chBF regulation in the normal retina, and rBF and chBF dysregulation in disease states. Quantitative BF measurement affords a comparison of BF changes between experimental groups, facilitating early detection and the monitoring of treatment efficacy. In addition, because MRI is noninvasive, this technique could potentially be used in human applications. However, much work remains to be performed before clinical applications can be realized. This technique could provide a valuable tool to study animal models of retinal diseases. Future studies will include a comparison of BF MRI with other BF measurement techniques (such as microspheres), and an investigation of the layer-specific retinal and choroidal responses to physiological and visual stimulation, as well as disease states.

Abbreviations used

ASL	arterial spin labeling
BF	blood flow
BOLD fMRI	blood oxygenation level-dependent functional MRI
chBF	choroidal blood flow
EPI	echo planar imaging
rBF	retinal blood flow

SD standard deviation

Acknowledgments

This work was supported in part by the National Eye Institute/National Institutes of Health (R01 EY018855 and R01 EY014211) and the Department of Veterans Affairs (VA MERIT Award). ERM was supported in part by National Institutes of Health T32EB005969.

REFERENCES

1. Cioffi, GA.; Granstam, E.; Alm, A. Ocular Circulation. In: Kaufman, PL.; Alm, A., editors. Adler's Physiology of the Eye. 10th ed.. St. Louis, MO: Mosby; 2003. p. 747-773.
2. Cheng H, Nair G, Walker TA, Kim MK, Pardue MT, Thule PM, Olson DE, Duong TQ. Structural and functional MRI reveals multiple retinal layers. Proc. Natl. Acad. Sci. USA 2006q;103:17,525–17,530.
3. Chen J, Wang Q, Zhang J, Yang X, Wang J, Berkowitz BA, Wickline SA, Song SK. In vivo quantification of T1, T2, and apparent diffusion coefficient in the mouse retina at 11.74T. Magn. Reson. Imaging 2008;59:731–738.
4. Roth S. The effects of halothane on retinal and choroidal blood flow in cats. Anesthesiology 1992;76:455–460. [PubMed: 1539858]
5. Tilton RG, Chang K, Weigel C, Eades D, Sherman WR, Kilo C, Williamson JR. Increased ocular blood flow and ^{125}I-albumin permeation in galactose-fed rats: inhibition by sorbinil. Invest. Ophthalmol. Vis. Sci 1988;29:861–868. [PubMed: 3372163]
6. Riva CE, Cranstoun SD, Grunwald JE, Petrig BL. Choroidal blood flow in the foveal region of the human ocular fundus. Invest. Ophthalmol. Vis. Sci 1994;35:4273–4281. [PubMed: 8002247]
7. Wang L, Grant C, Fortune B, Cioffi GA. Retinal and choroidal vasoreactivity to altered $PaCO_2$ in rat measured with a modified microsphere technique. Exp. Eye Res 2008;86:908–913. [PubMed: 18420196]
8. Ahmed J, Pulfer M, Linsenmeier RA. Measurement of blood flow through the retinal circulation of the cat during normoxia and hypoxemia using fluorescent microspheres. Microvasc. Res 2001;62:143–153. [PubMed: 11516243]
9. Nilsson SFE, Maepea O, Alm A, Narfstrom K. Ocular blood flow and retinal metabolism in Abyssinian cats with hereditary retinal degeneration. Invest. Ophthalmol. Vis. Sci 2001;42:1038–1044. [PubMed: 11274083]
10. Clermont AC, Brittis M, Shiba T, McGovern T, King GL, Bursell SE. Normalization of retinal blood flow in diabetic rats with primary intervention using insulin pumps. Invest. Ophthalmol. Vis. Sci 1994;35:981–990. [PubMed: 8125761]
11. Pemp B, Schmetterer L. Ocular blood flow in diabetes and age-related macular degeneration. Can. J. Ophthalmol 2008;43:295–301. [PubMed: 18443612]
12. Tilton RG, Chang KC, LeJeune WS, Stephan CC, Brock TA, Williamson JR. Role for nitric oxide in the hyperpermeability and hemodynamic changes induced by intravenous VEGF. Invest. Ophthalmol. Vis. Sci 1999;40(3):689–696. [PubMed: 10067972]
13. Lin J, Roth S. Ischemic preconditioning attenuates hypoperfusion after retinal ischemia in rats. Invest. Ophthalmol. Vis. Sci 1999;40(12):2925–2931. [PubMed: 10549654]
14. Cheng H, Yan Y, Duong TQ. Temporal statistical analysis of laser speckle image and its application to retinal blood-flow imaging. Optics Express 2008;16:10,214–10,219.
15. Preussner PR, Richard G, Darrelmann O, Weber J, Kreissig I. Quantitative measurement of retinal blood flow in human beings by application of digital image-processing methods to television fluorescein angiograms. Graefes Arch. Clin. Exp. Ophthalmol 1983;221:110–112. [PubMed: 6689414]
16. Szkulmowska A, Szkulmowski M, Szlag D, Kowalczyk A, Wojtkowski M. Three-dimensional quantitative imaging of retinal and choroidal blood flow velocity using joint spectral and time

domain optical coherence tomography. Optics Express 2009;17:10,584–10,598. [PubMed: 20052085]

17. Sicard K, Shen Q, Brevard ME, Sullivan R, Ferris CF, King JA, Duong TQ. Regional cerebral blood flow and BOLD responses in conscious and anesthetized rats under basal and hypercapnic conditions: implications for functional MRI studies. J. Cereb. Blood Flow Metab 2003;23(4):472–481. [PubMed: 12679724]
18. Shen Q, Cheng H, Pardue MT, Chang TF, Nair G, Vo VT, Shonat RD, Duong TQ. Magnetic resonance imaging of tissue and vascular layers in the cat retina. J. Magn. Reson. Imaging 2006;23(4):465–472. [PubMed: 16523482]
19. Berkowitz BA, Roberts R, Goebel DJ, Luan H. Noninvasive and simultaneous imaging of layer-specific retinal functional adaptation by manganese-enhanced MRI. Invest. Ophthalmol. Vis. Sci 2006;47:2668–2674. [PubMed: 16723485]
20. Li Y, Cheng H, Duong TQ. Blood-flow magnetic resonance imaging of the retina. Neuroimage 2008;39:1744–1751. [PubMed: 18063388]
21. Li Y, Cheng H, Shen Q, Kim M, Thule PM, Olson DE, Pardue MT, Duong TQ. Blood-flow magnetic resonance imaging of retinal degeneration. Invest. Ophthalmol. Vis. Sci 2009;50:1824–1830. [PubMed: 18952917]
22. Muir ER, Shen Q, Duong TQ. Cerebral blood flow MRI in mice using the cardiac-spin-labeling technique. Magn. Reson. Med 2008;60(3):744–748. [PubMed: 18727091]
23. Matta BF, Heath KJ, Tipping K, Summors AC. Direct cerebral vasodilatory effects of sevoflurane and isoflurane. Anesthesiology 1999;91:677–680. [PubMed: 10485778]
24. Sinclair MD. A review of the physiological effects of alpha2-agonists related to the clinical use of medetomidine in small animal practice. Can. Vet. J 2003;44:885–897. [PubMed: 14664351]
25. Lei H, Grinberg O, Nwaigwe CI, Hou HG, Williams H, Swartz HM, Dunn JF. The effects of ketamine–xylazine anesthesia on cerebral blood flow and oxygenation observed using nuclear magnetic resonance perfusion imaging and electron paramagnetic resonance oximetry. Brain Res 2001;913:174–179. [PubMed: 11549383]
26. Herscovitch P, Raichle ME. What is the correct value for the brain–blood partition coefficient for water? J. Cereb. Blood Flow Metab 1985;5:65–69. [PubMed: 3871783]
27. Nair G, Shen Q, Duong TQ. Relaxation time constants and apparent diffusion coefficients of rat retina at 7 Tesla. Int. J. Imaging Syst. Technol 2010;20:126–130.
28. Duong TQ, Muir ER. Magnetic Resonance Imaging of the Retina. Jpn. J. Ophthalmol 2009;53:352–367. [PubMed: 19763752]
29. Stefansson E, Wilson CA, Lightman SL, Kuwabara T, Palestine AG, Wagner HG. Quantitative measurements of retinal edema by specific gravity determinations. Invest. Ophthalmol. Vis. Sci 1987;28:1281–1289. [PubMed: 3610546]
30. Schmucker C, Schaeffel F. A paraxial schematic eye model for growing C57BL/6 mouse. Vision Res 2004;44:1857–1867. [PubMed: 15145680]
31. Gabhann FM, Demetriades AM, Deering T, Packer JD, Shah SM, Duh E, Campochiaro PA, Popel AS. Protein transport to choroid and retina following periocular injection: theoretical and experimental study. Ann. Biomed. Eng 2007;35:615–630. [PubMed: 17277991]
32. Spaide RF, Koizumi H, Pozonni MC. Enhanced depth imaging spectral-domain optical coherence tomography. Am. J. Ophthalmol 2008;146:496–500. [PubMed: 18639219]
33. Ramrattan RS, van der Schaft TL, Mooy CM, de Bruijn WC, Mulder PGH, de Jong PTVM. Morphometric analysis of Bruch's membrane, the choriocapillaries, and the choroid in aging. Invest. Ophthalmol. Vis. Sci 1994;35:2857–2864. [PubMed: 8188481]
34. Johnson GL. Contributions to the comparative anatomy of vertebrates, chiefly based on ophthalmoscopic examination. Philos. Trans. R. Soc. London, B 1901;194:1–82.
35. Wang L, Fortune B, Cull G, McElwain KM, Cioffi GA. Microspheres method for ocular blood flow measurement in rats: size and dose optimization. Exp. Eye Res 2007;84:108–117. [PubMed: 17069799]
36. Friedman E, Kopald HH, Smith TR. Retinal and choroidal blood flow determined with krypton 85 in anesthetized animals. Invest. Ophthalmol 1964;3:539–547. [PubMed: 14229941]

37. Chiou GCY, Chen YJ. Effects of D- and L-isomers of timolol on retinal and choroidal blood flow in ocular hypertensive rabbit eyes. J. Ocular Pharm 1992;8:183–190.

38. Keough EM, Wilcox LM, Connolly RJ, Hotte CE. The effect of complete tenotomy on blood flow to the anterior segment of the canine eye. Invest. Ophthalmol. Vis. Sci 1980;19(11):1355–1359. [PubMed: 7429770]

39. Steinle JJ, Krizsan-Agbas D, Smith PG. Regional regulation of choroidal blood flow by autonomic innervation in the rat. Am. J. Physiol. Regul. Integr. Comp. Physiol 2000;279:202–209.

40. Laties AM, Jacobowitz DA. A comparative study of the autonomic innervation of the eye in monkey, cat and rabbit. Anat. Rec 1966;156:383–396. [PubMed: 4960396]

41. Alm A. The effect of sympathetic stimulation on blood flow through the uvea, retina and optic nerve in monkeys. Exp. Eye Res 1977;25:19–24. [PubMed: 408161]

42. Yu D-Y, Cringle SJ, Su E-N, Yu PK. Intraretinal oxygen levels before and after photoreceptor loss in the RCS rat. Invest. Ophthalmol. Vis. Sci 2000;41:3999–4006. [PubMed: 11053305]

43. Small KW, Stefansson E, Hatchell DL. Retinal blood flow in normal and diabetic dogs. Invest. Ophthalmol. Vis. Sci 1987;28(4):672–675. [PubMed: 3557871]

44. Pouliot M, Deschenes MC, Hetu S, Chemtob S, Lesk MR, Couture R, Vaucher E. Quantitative and regional measurement of retinal blood flow in rats using N-isopropyl-p-[^{14}C]-iodoamphetamine ([^{14}C]-IMP). Exp. Eye Res 2009;89:960–966. [PubMed: 19698709]

45. Yu DY, Alder VA, Cringle SJ. Measurement of blood flow in rat eyes by hydrogen clearance. Am. J. Physiol 1991;261:H960–H968. [PubMed: 1887939]

46. Stefansson E, Wagner HG, Seida M. Retinal blood flow and its auto-regulation measured by intraocular hydrogen clearance. Exp. Eye Res 1988;47:669–678. [PubMed: 3197768]

47. Yu DY, Alder VA, Cringle SJ, Brown MJ. Choroidal blood flow measured in the dog eye in vivo and in vitro by local hydrogen clearance polarography – validation of a technique and response to raised intraocular pressure. Exp. Eye Res 1988;46:289–303. [PubMed: 3350072]

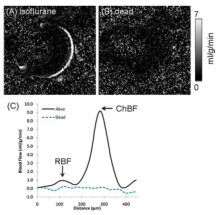

Figure 1.
(A) Layer-specific blood flow image from a mouse under 1.1% isoflurane. (B) Blood flow acquired in a dead mouse in the same setting (same animal). Scale bar indicates blood flow values from 0 to 7 mL/g/min. (C) Blood flow profiles from the images in (A) and (B). chBF, choroidal blood flow; rBF, retinal blood flow.

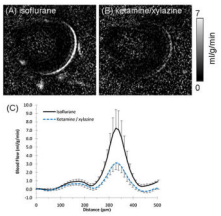

Figure 2.
Blood flow images in a mouse under 1.1% isoflurane (A) and ketamine/xylazine (100 mg/kg–10 mg/kg) (B). Scale bar indicates blood flow values from 0 to 7 mL/g/min. (C) Group-average blood flow profiles across the retinal thickness under either isoflurane or ketamine/xylazine from the same animals (n = 4, error bars show standard deviation).

Table 1

Blood flow peak values (mL/g/min) of the retinal (rBF) and choroidal (chBF) layers under isoflurane or ketamine/xylazine (n = 7, mean ± SD)

	rBF	chBF	chBF: rBF
Isoflurane	1.3 ± 0.44[a,c]	7.7 ± 2.1[b,c]	6.3 ± 1.9
Ketamine/xylazine	0.88 ± 0.22[a,d]	4.3 ± 1.9[b,d]	4.8 ± 1.2
Difference (%)	−29 ± 17	−42 ± 23	

[a] $p < 0.01$.

[b] $p < 0.01$.

[c] $p < 0.01$.

[d] $p < 0.01$.

Table 2

Thicknesses (μm) of the retinal vascular layer, avascular layer and choroidal vascular layer, total thickness and peak-to-peak distance between retinal and choroidal vasculatures. There were no statistically significant differences between the anesthetics in any of these parameters

	Retinal layer	Avascular layer	Choroidal layer	Total thickness	Peak-to-peak distance
Isoflurane	77 ± 24	94 ± 13	78 ± 3	249 ± 19	170 ± 18
Ketamine/xylazine	84 ± 26	87 ± 6	78 ± 10	249 ± 28	161 ± 17

NMR Biomed. Author manuscript; available in PMC 2011 February 25.

Table 3

Reported values of retinal, choroidal and cerebral blood flow (rBF, chBF and CBF, respectively) in mL/g/min, except where noted

Reference	Method	Animal	Anesthesia	rBF	chBF	CBF
(1)	Microspheres	Monkey		0.48	18.98	0.78
(8)	Microspheres	Cat	Urethane	0.198		
(9)[a]	Microspheres	Cat	α-Chloralose	0.141	7.46	
(4)	Microspheres	Cat	Halothane	0.54	13.09	0.69
(5)	Microspheres	Rat	Inactin	0.44	1.42[b]	0.58
(12)	Microspheres	Rat	Thiopental	0.4	3.8[b]	0.58
(13)	Microspheres	Rat	Halothane[c]	0.22	1.45[b]	
(38)	Microspheres	Dog	Pentobarbital	0.12	9.61	
(43)	Microspheres	Dog	Pentobarbital/succinylcholine	0.91		
(44)	^{14}C-IMP	Rat	Awake	0.92		0.97
(36)	Krypton-85	Cat	Pentobarbital	1.66	12	
(45)	Hydrogen clearance	Rat	Inactin	3.73		
(46)	Hydrogen clearance	Cat	α-Chloralose	0.56		
(47)	Hydrogen clearance	Dog	Pentobarbital/thiopental		2–4	

[a] Values reported as g/g/min. Given that the blood density is 1.06 g/mL (26), values in units of g/g/min and mL/g/min are essentially equal.

[b] Values are of the combined choroid and sclera, probably reducing the quantitative value substantially.

[c] Ketamine/xylazine were also given during surgery, and may have had a lingering effect on blood flow.